Three-Dimensional Simulation of a Magnitude 7.75 Earthquake on the San Andreas Fault

Kim B. Olsen, Ralph J. Archuleta,* Joseph R. Matarese

Simulation of 2 minutes of long-period ground motion in the Los Angeles area with the use of a three-dimensional finite-difference method on a parallel supercomputer provides an estimate of the seismic hazard from a magnitude 7.75 earthquake along the 170-kilometer section of the San Andreas fault between Tejon Pass and San Bernardino. Maximum ground velocities are predicted to occur near the fault (2.5 meters per second) and in the Los Angeles basin (1.4 meters per second) where large amplitude surface waves prolong shaking for more than 60 seconds. Simulated spectral amplitudes for some regions within the Los Angeles basin are up to 10 times larger than those at sites outside the basin at similar distances from the San Andreas fault.

The damage in Mexico City from the Michoacan earthquake (19 September 1985) and in the Marina district of San Francisco from the Loma Prieta earthquake (19 October 1989) has clearly illustrated the risks for population centers located in basins at a significant distance from the causative fault. The sediments filling the basins, which have low elastic moduli, amplify the seismic waves relative to the surrounding bedrock. In addition, the edges of the basins can generate large-amplitude waves that can prolong the shaking in the basins. Moderate-sized events, such as the magnitude (**M**) 6.7 Northridge earthquake (17 January 1994), the **M** 6.0 Whittier Narrows earthquake (1 October 1987), and the **M** 6.6 San Fernando earthquake (9 February 1971), have emphasized the seismic hazard from faults on the Los Angeles (LA) fault system (*1*–*5*). Nonetheless, the San Andreas fault (SAF) remains potentially the most hazardous for the LA area because it has produced large earthquakes in historical time (*2*, *6*, *7*).

To determine the amount of shaking that could occur in the LA area, we simulated a **M** 7.75 earthquake on the section of the SAF closest to LA. We considered a propagating rupture for 170 km from Tejon Pass to San Bernardino (Fig. 1A). This part of the SAF, which consists of two segments, the Mojave and part of the San Bernardino Mountains segment (*2*), is believed to have produced the **M** 7.5 earthquake on 12 December 1812 (*6*, *8*). The average recurrence time between large earthquakes with surface rupture on the Mojave segment is 150^{+123}_{-71} years and on the San Bernardino segment it is 146^{+91}_{-60} years (*2*). Mean conditional probabilities of 26 ± 11% (**M** 7.53) and 28 ± 13% (**M** 7.30) have been determined for earthquakes on the Mojave and San Bernardino segments, respectively, to occur before the year 2024 (*2*). Because both segments have similar recurrence intervals and conditional probabilities, and may have ruptured together in earlier events (*6*), it is reasonable to consider a scenario where this section of the SAF ruptures again in a single earthquake.

To estimate the ground shaking from such an earthquake (*9*) we incorporated the three-dimensional (3D) structure of the medium through which the seismic waves will travel from the SAF to LA. The geology of this region is varied: Igneous and metamorphic basement rocks crop out extensively in the Mojave Desert and San Gabriel Mountains (*10*) whereas sedimentary rocks fill the deep basins in LA and the San Fernando Valley (*11*). The seismic energy will thus propagate for at least 35 km through igneous and metamorphic rocks before impinging on the sedimentary basins of greater LA (Fig. 1B). Were it not for the basins beneath the San Fernando Valley and LA (including the San Gabriel Valley) (Fig. 1B), the model would consist of horizontal layers where the material parameters varied only with depth (*12*). However, with their irregular geometry and different material properties, these sedimentary basins affect the ground motion by amplifying seismic waves, prolonging their duration, and generating waves at the basin edges (*3*, *13*, *14*).

To approximate a **M** 7.75 earthquake on the SAF, we simulated a rupture on a fault plane 16.5 km deep and 170 km long that extends from Quail Lake (10 km southeast of Gorman) to Mill Creek (11 km northeast of Redlands). The fault plane had a constant strike (118°) that followed the strike of the SAF with a slight deviation (maximum of 6 km) at the northwestern end of the Mojave segment (Fig. 1A). The rupture initiated at a point 2 km from the northwestern end of the fault segment, at 10 km depth, and dextrally offset the two sides of the fault by 4.82 m everywhere (*15*) (Table 1). The earthquake rupture lasted 68 s before terminating at Mill Creek. The shear (S) waves that continuously radiated from the rupture impinged on the basins about 20 s after the earthquake started. Some areas of the LA basin continued to vibrate for more than 60 s because of the continual stimulation from waves arriving from different parts of the fault, waves generated at the basin edges, and resonances in the basin.

Numerical model for the earthquake rupture and 3D wave propagation. We subdivided a large volume (230 km by 140.4 km by 46 km) of southern California into 23,209,875 cubes 0.4 km on a side with a gridpoint at each vertex. Each gridpoint was assigned a compressional wave velocity, an S wave velocity, and a density (*16*). The 3D structure did not include the basins beneath the Upper Santa Ana Valley, the San Bernardino Valley, or the Ventura area (*14*, *17*) because there was no discretized 3D model for their elastic and material properties. Therefore the amplitude and duration of the simulated ground motion is probably underestimated in these areas (*14*, *18*).

We kinematically simulated the earthquake as a constant slip that radially propagated outward with a velocity 85% of the local S wave velocity. The slip rate function is Gaussian with a dominant period of 4.5 s. This function was later deconvolved from the synthetic records to obtain a slip rate with uniform spectral response to displacement for frequencies up to 0.4 Hz that is constant everywhere on the fault (*3*). This formulation allows the seismic moment and synthetics to be scaled by a single value of slip. The effective rise time is about 3 s everywhere on the fault (*19*).

The source was implemented in the finite-difference grid by adding $-M_{ij}(t)/V$ to $S_{ij}(t)$, where $M_{ij}(t)$ is the ij'th component of the moment tensor for the earthquake, V is

Table 1. Earthquake rupture parameters.

Southeast fault limit	34.089°N, 117.064°W
Northwest fault limit	34.808°N, 118.688°W
Hypocenter	34.800°N, 118.669°W
Hypocenter depth (km)	10
Slip (m)	4.82
Moment magnitude (**M**)	7.75
Width, length (km)	16, 170
Depth to top of fault (km)	0.5
Dip, strike, rake (°)	90, 118, 180

K. B. Olsen is at the Institute for Crustal Studies, University of California, Santa Barbara, CA 93106, USA. R. J. Archuleta is in the Department of Geological Sciences and Institute for Crustal Studies, University of California, Santa Barbara, CA 93106, USA. J. R. Matarese is at the Earth Resources Laboratory, Department of Earth, Atmospheric and Planetary Sciences, Massachusetts Institute of Technology, Cambridge, MA 02142, USA.

*To whom correspondence should be addressed.

Reproduced with permission of the copyright owner. Further reproduction prohibited without permission.

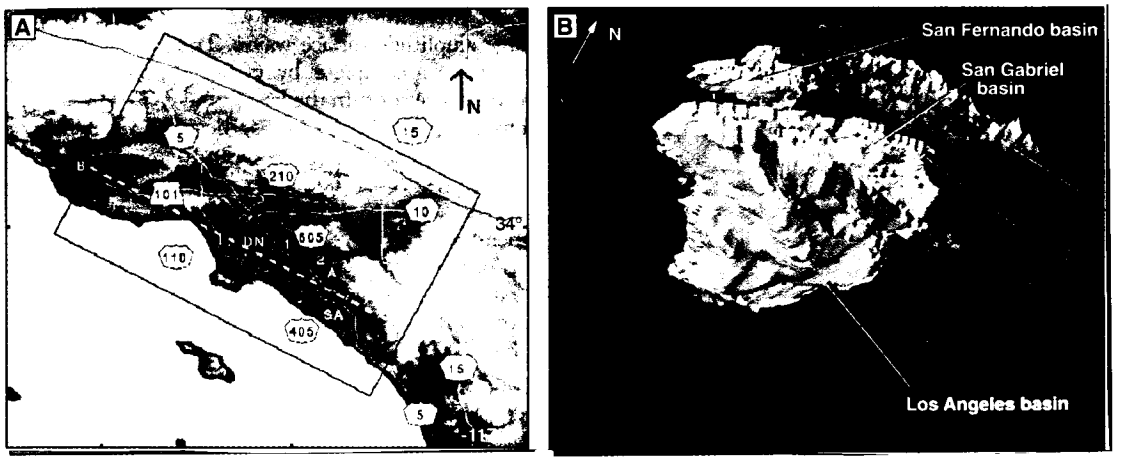


Fig. 1. (**A**) Topographic map of southern California. The rectangle shows the areal extent of the simulation. The SAF is shown by the green line; our approximation to the SAF is shown by the dashed white line. The thick solid white line is the coastline of southern California. The thin white lines depict major freeways. The dashed white line B-B′ is a profile used for displaying seismograms. 1, 2, and 3 denote sites in the basin, on the edge of the basin, and outside the basin, respectively. A, Anaheim; CP, Compton; DN, Downey; HB, Huntington Beach; IN, Inglewood; SA, Santa Ana; and SM, Santa Monica. (**B**) Three-dimensional perspective of the isosurface for an S-wave velocity of 2.6 km/s illustrating the geometry of the basins. Vertical exaggeration is 3.2. Modeling parameters are listed in Table 1.

the cell volume, and $S_{ij}(t)$ is the ij'th component of the stress tensor on the fault at time t (Table 2).

We use a staggered-grid finite-difference scheme to solve the 3D elastic equations of motion (*20*); the accuracy is fourth order in space and second order in time. The numerical implementation of the 3D scheme is described in (*21*). To eliminate artificial reflections from the boundaries of the grid, we implemented absorbing boundary conditions coupled with a buffer zone of strong attenuation (*22*). In the following, we removed these zones and present the simulation results within the area (174 km by 114.8 km) (Fig. 1A) that encompasses the population centers of the LA area.

Finite-difference modeling of elastic waves in large-scale 3D models, such as the one used in the SAF simulation, consumes vast quantities of computational resources. The earth model and the calculated stress and velocity fields require gigabytes of physical memory and gigaflops of CPU for tens of hours to simulate the total duration of ground motion within a reasonable period of time. Such computational requirements are beyond the resources of workstations and most supercomputers with shared-memory configurations. To carry out our simulation we used grid-decomposition techniques on the massively parallel processors of the nCUBE 2 at the Earth Resources Laboratory of the Massachusetts Institute of Technology.

Table 2. Three-dimensional modeling parameters.

Spatial discretization (km)	0.4
Temporal discretization (s)	0.025
Minimum P-wave velocity (km/s)	2.41
Minimum S-wave velocity (km/s)	1.00
Minimum density (kg/m^3)	2070
Gridpoints along 118°	576*
Gridpoints along 28°	352*
Gridpoints along vertical	116
Timesteps	4800
Simulation time (s)	120

*Figures show 436 gridpoints along the 118° azimuth and 288 gridpoints along the 28° azimuth.

Figure 2 illustrates how we subdivide the 3D volume of the model over eight parallel processors (Fig. 2). Each processor is responsible for performing stress and velocity calculations for its portion of the grid, as well as dealing with boundary conditions at the external edges of each volume. At the internal edges, where neighboring portions of the earth volume are contained on separate nodes, the processors must exchange stress and velocity information to propagate the waves correctly. On the nCUBE 2, this communication time represents a negligible part of the total run time. In other words, the same simulation can be performed twice as fast on twice as many processors as long as the internal edges represent a small part of the model held by each processor.

For the SAF simulation we used all 512 processors available on the nCUBE 2. With grid dimensions of 576 by 352 by 116 points, the most memory-efficient decomposition involved assigning subgrids of 36 by 44 by 29 points to the individual processors. In keeping with the fourth order finite-difference scheme, a two-point-thick padding layer was added to the outside of each subgrid to bring the total subgrid dimensions to 40 by 48 by 33 points. To store 12 arrays (three elastic coefficients, three components of velocity, and six components of stress) of this size required just over 2.9 megabytes of the 4 megabytes of physical memory on each processor. The remaining memory was consumed by the program logic and additional variables as well as the operating system kernel. Using a grid decomposition code based upon the portable Message Passing Interface standard, the finite-difference simulation took 17 s per timestep or nearly 23 hours to complete the 120 s of simulated ground motion. More than a gigabyte of disk space was used to store the time history of the ground motion at the surface.

Simulated ground motion and seismic hazard in LA. To illustrate the development of the ground motion as the rupture propagated along the SAF we show snapshots of long-period ground velocity (Fig. 3) over the 19,975 km^2 area (Fig. 1A). By 20 s, the S waves had entered San Fernando Val-

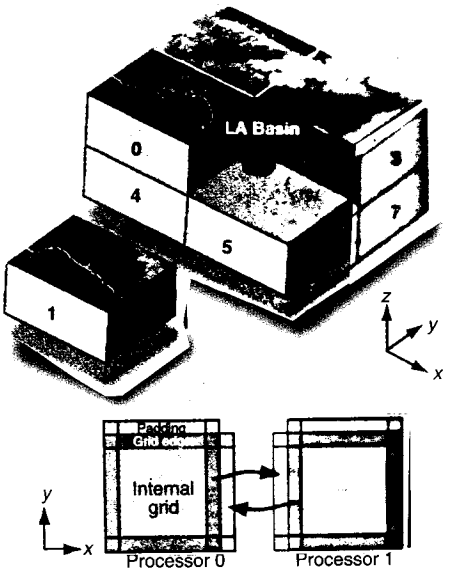


Fig. 2. Grid decomposition of the SAF rupture model on the nCUBE 2. (**Top**) The model is decomposed into a number of subgrids, labeled 0 through 7. The actual model was divided into 512 subgrids, corresponding to the number of processors used in the simulation. (**Bottom**) Illustration of the communication between neighboring subgrids. The fourth-order finite-difference scheme requires that a two-point-thick padding layer be added to the outside of each subgrid in order to propagate the waves correctly. This padding layer always contains the most recently updated wavefield parameters exchanged from the edge of the neighboring subgrid (arrows).

Reproduced with permission of the copyright owner. Further reproduction prohibited without permission.

ley. By 30 s, when the rupture had propagated about halfway along the SAF, the S waves had entered the main LA basin. The area near the northern intersection of Interstates 5 and 405 showed intense ground motion. The high intensity was produced because resonance in the deep part of the San Fernando Valley basin radiated secondary waves as seen by the faint circular wavefronts centered on this area (R, Fig. 3 at 40 s). At 40 s, the ground motion in the LA basin had intensified: the San Gabriel Valley, just southeast of the intersection of Interstates 10 and 605, and the area just south of downtown LA show large amplitude ground motions. At 50 s the entire LA basin was excited by large amplitude surface waves. The rupture was almost complete by 60 s, at which time the wavefronts in the basin slowly began changing direction from southeast parallel to the long axis of the LA basin to the southwest. At 70 s, large amplitude waves were generated by reflections from the steep northeast sides of the basin; the peaks and troughs of the waves were aligned with the long axis of the basin and propagated west into the offshore area. This pattern persisted but diminished through 100 s where only faint shadows mimicked the larger amplitudes that existed 30 s before.

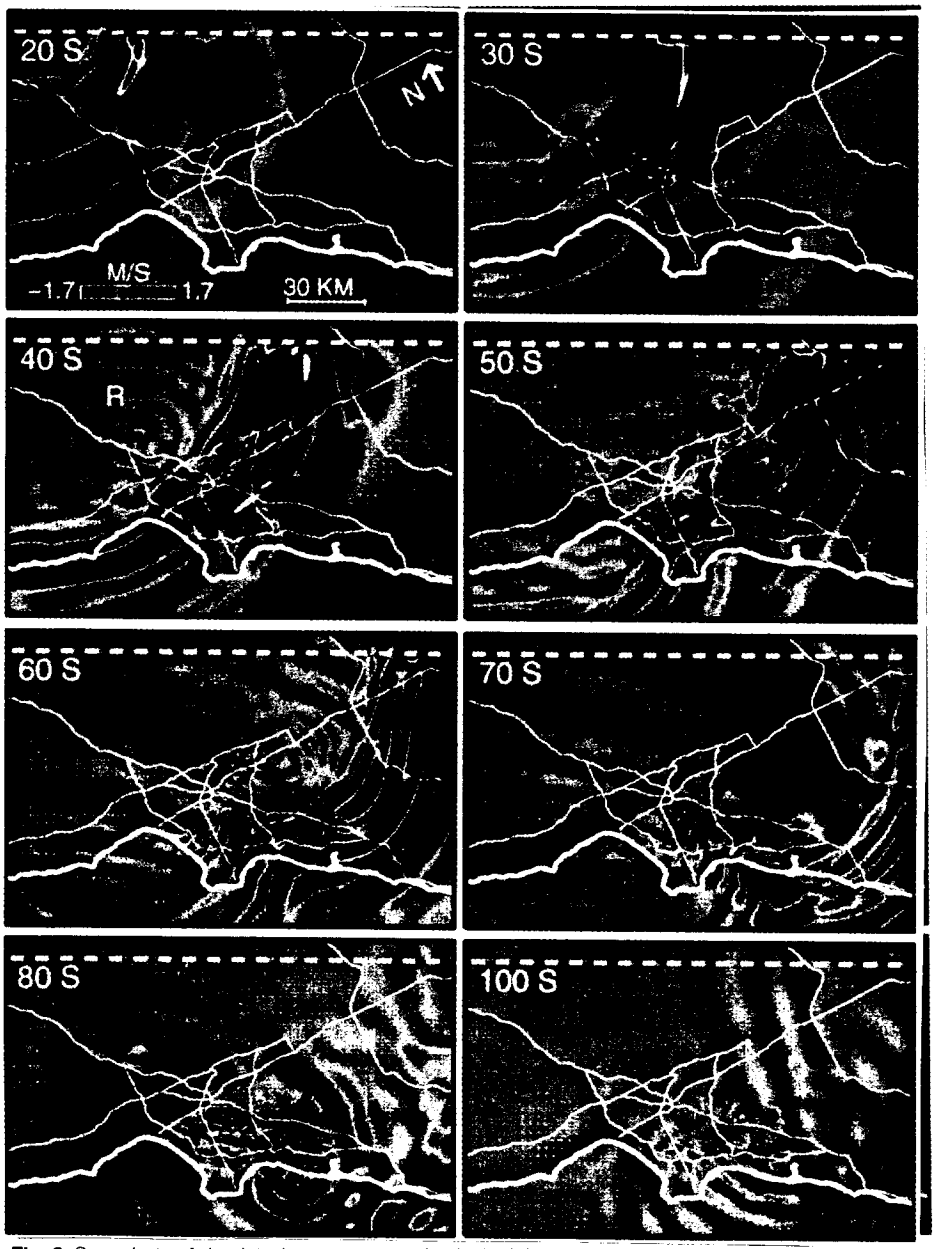


Fig. 3. Snapshots of simulated wave propagation in the LA area for the hypothetical SAF earthquake; the snapshots depict the horizontal (118°) particle velocities that represent shaking parallel to the SAF (*23*) from 20 s to 100 s after the origin time of the rupture. Red depicts large amplitudes of both positive and negative polarity. R depicts an area of local resonance above the deepest part of the San Fernando Valley basin. The particle motion is scaled by a constant for all snapshots. Lines labeled as in Fig. 1A.

To encapsulate many of these effects we show a suite of seismograms and the S wave velocity structure (Fig. 4, A and B) from the Ventura basin to the mountains east of San Clemente (B-B′, Fig. 1A). By visually correlating the suite of seismograms with the S wave velocity structure, the effect of the basin on the amplitude and duration of shaking is evident. The basin affected all three components of motion (Fig. 4C) but primarily the component parallel (118°) to the axis of the trough (*23*). To examine the frequency content of the shaking, we compared the Fourier spectral amplitudes of particle velocity for the 118° component for three sites (Fig. 4D): (i) over the deepest part of the basin, (ii) above the edge of the basin, and (iii) outside the basin (Fig. 1A). The maximum spectral amplitude for the edge site was a factor of two larger than for the site over the deepest part of the basin. The edge site had its spectral maximum at a higher frequency (0.25 Hz) compared to the site above the central basin where the first broad peak occurred around 0.16 Hz—approximately the fundamental resonant frequency of the LA basin (*24*). The spectral amplitude for a site at the edge of the basin was 10 times the spectral amplitude for a site outside the basin even though both are at the same distance from the SAF (*25*).

Contours of the peak particle velocity over the area reveal effects due to rupture and structure (Fig. 5). The 118° component was largest near the SAF and in the LA basin. The high amplitudes near the fault were expected; the amplitudes (>0.5 m/s) in the LA basin ~60 km from the fault were not. The 0.25 m/s contour basically outlines the San Gabriel Valley and LA basins. Moreover, there is a large area with amplitudes larger than 0.75 m/s corresponding to the deeper parts of the LA basin.

The large lobe with peak velocity greater than 0.75 m/s for the 28° component (Fig. 5) reflects the directivity of the rupture (*4*, *26*) and the radiation pattern from the source (*23*) that combine to produce the maximum slip velocity 2.5 m/s. The 28° component shows that in the simulation those areas in the forward direction of the rupture were as severely shaken as LA. Most of the area with peak velocity greater than 0.75 m/s was confined to the less populated San Gabriel Mountains. However, the southeastern part of the 0.75 m/s lobe cov-

Table 3. Comparison of maximum peak particle velocities (m/s) near the SAF and in the LA basin for three components of wave motion.

Location	118°	28°	Vertical
Near SAF	2.01	2.51	0.91
LA basin	1.37	0.70	0.54

Reproduced with permission of the copyright owner. Further reproduction prohibited without permission.

ered the region in the populated Upper Santa Ana Valley (including cities such as Ontario, Pomona, and Upland) and the San Bernardino Valley (including cities such as San Bernardino and Redlands). Because the SAF passes just to the northwest of these areas, the severity of the shaking increases because of proximity to the fault (*25*) and rupture directivity. The amplitude of the waves attenuated with distance from the SAF except for the amplification resulting from the LA basin where amplitudes on the 28° component also exceeded 0.5 m/s.

The smallest peak particle velocities were for the vertical component as expected for strike-slip motion on a vertical fault. However, like the horizontal components, the LA basin amplifies the vertical motion relative to the surrounding area. The net result is that the total ground motion in the LA region in the simulation was much larger than would be predicted by a 1D model (*3*, *13*, *14*). We illustrate this point by mapping the total cumulative kinetic energy (*27*) that takes into account the amplitude and duration of shaking for all three components of motion (Fig. 6). A large swath within 30 km of the SAF experienced significant shaking. The cumulative kinetic energy decreased with distance from the fault except for the basins, especially the LA basin—where, for frequencies up to 0.4 Hz, the cumulative kinetic energy was equivalent to that near the fault. The expected attenuation with distance of the amplitude of the seismic waves (*25*) was counteracted by the basin geometry and velocity structure.

The simulated ground motion should be considered in the context of three factors: (i) Because of computational limitations, the maximum frequency was 0.4 Hz. Observed ground motions contain higher frequencies that will increase the amplitudes of the particle velocities especially near the SAF where anelastic material attenuation has less effect than for distances far from the fault (*25*). The component of motion perpendicular to the strike (28°), is 25% larger than the parallel component near the fault (Table 3). This 28° component is amplified by directivity of the rupture and almost always has the maximum particle velocity (*4*, *26*). However, the observed near-fault peak velocities were generally associated with pulses dominated by frequencies 1.0 Hz or less (*4*, *26*) so that the lower frequency of 0.4 Hz may not be a critical factor. The structures most affected by the computed ground motion would be those that have their lowest mode response with frequencies less than 0.4 Hz (periods ≥2.5 s); almost all one- and two-story structures have their peak response at much higher frequencies (*28*). (ii) The minimum S wave velocity is 1.0 km/s, again due to computational limitations. In engineering terms this means that all of the ground motion is for rock rather than soil (*29*). Inclusion of the lower velocity sediments would increase the ground motion amplitudes (*30*). The omission of higher frequencies and lower near-surface velocities in the simulation define our results as a lower bound for the expected ground motion for the SAF rupture scenario. (iii) Our kinematic rupture model is smooth in that the slip and slip rate are constant everywhere on the fault and rupture velocity is a fixed percentage of the S wave velocity. The slip and the slip rate have plausible values (*15*) but could certainly be allowed to vary spatially; such variation would affect signal duration more than amplitude (*9*). In real, large earthquakes rupture velocity varies significantly over long fault length. A variable rupture velocity would decrease the coherency of the waves leaving the fault and mitigate the effects of directivity. Whether this would increase or decrease the ground motion in LA is unknown.

Our simulation of a M 7.75 earthquake on the SAF predicted long-period peak par-

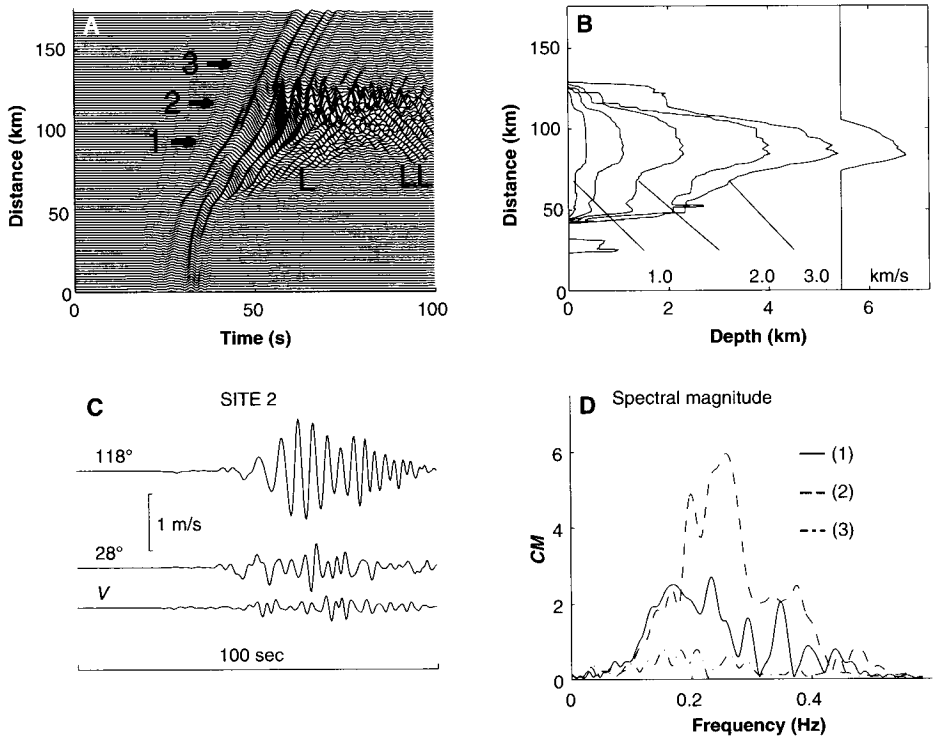


Fig. 4. Seismic response along profile B-B′ (see Fig. 1A) for the hypothetical SAF earthquake. (**A**) Simulated velocity seismograms for the 118° horizontal component: site 1 is within the basin, site 2 is along the basin edge, and site 3 is outside the basin. (**B**) Vertical cross section along B-B′; the contours on the map depict the S-wave velocity at a contour interval of 0.5 km/s. (**C**) Three component velocity seismograms at site 2. L depicts Love waves and LL depicts Love waves reflected at the basin edge. (**D**) Fourier spectral amplitude for the 118° horizontal component at sites 1, 2, and 3 (see Fig. 1A).

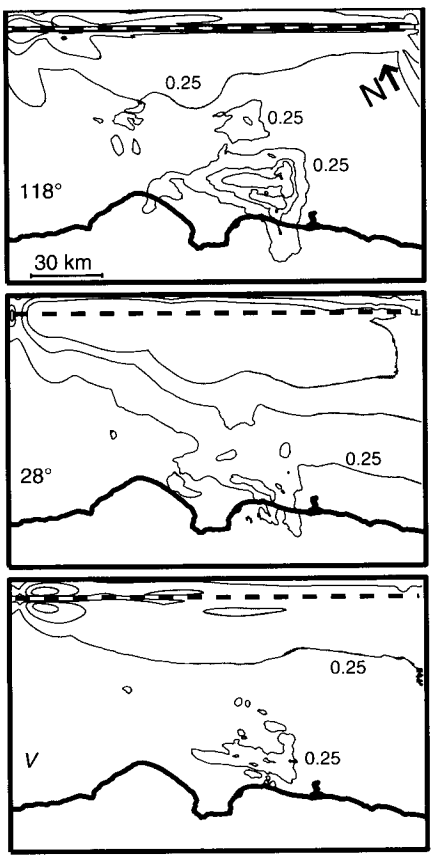


Fig. 5. Contour maps of simulated peak velocities along the 118°, 28°, and vertical components for the hypothetical SAF earthquake. Contour interval is 0.25 m/s with the 0.25 m/s contour labeled. Lines labeled as in Fig. 1A.

Reproduced with permission of the copyright owner. Further reproduction prohibited without permission.

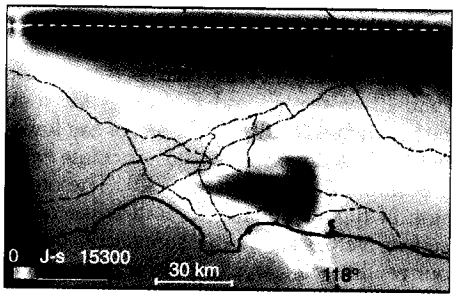


Fig. 6. Map of simulated total cumulative kinetic energies for the hypothetical SAF earthquake. Note that the color scale is logarithmic in units of Joules-seconds (J-s). Lines labeled as in Fig. 1A.

ticle velocities greater than 1.0 m/s at some areas in LA and greater than 0.75 m/s over a large central area even though the main trough of the basin is about 60 km from the fault (Fig. 5). These peak velocities are similar to those observed near the fault for some damaging earthquakes (*4*, *26*) and larger than particle velocities from simulated **M** 6.75 earthquakes on faults in LA (*3*). While these simulated long-period waves have large amplitudes, the threat they pose to existing structures is unknown.

REFERENCES AND NOTES

1. J. Dolan *et al.*, *Science* **267**, 199 (1995).
2. Working Group on California Earthquake Probabilities, *Bull. Seismol. Soc. Am.* **85**, 379 (1995).
3. K. Olsen and R. Archuleta, 3-D Simulation of Earthquakes on the Los Angeles Fault System, in preparation.
4. T. Heaton *et al.*, *Science* **267**, 206 (1995).
5. The moment magnitude, **M** = (2/3) log M_0 − 6.03 [T. Hanks and H. Kanamori, *J. Geophys. Res.* **84**, 2348 (1979)] was defined so that it may be uniformly applied to any earthquake. Seismic moment, $M_0 = \mu As$, is given in Nm [K. Aki, *Earthquake Res. Inst. Bull.* **44**, 73 (1966)] where μ is the shear modulus, A is the area of the fault over which slip has occurred, and s is the average slip over A. In our model the average material properties at the SAF are: density 2770 kg/m^3, shear modulus 3.62 × 10^{10} N/m^2 and shear wave velocity 3.59 km/s.
6. K. Sieh *et al.*, *J. Geophys. Res.* **94**, 603 (1989).
7. W. Ellsworth, *U.S. Geol. Surv. Prof. Pap. 1515* (1990), p. 153.
8. G. Jacoby *et al.*, *Science* **241**, 196 (1988).
9. Previous simulations of the great 1857 earthquake have estimated displacements for only a few locations in the LA area using a 1D velocity model [R. Butler and H. Kanamori, *Bull. Seismol. Soc. Am.* **70**, 943 (1980); M. Bouchon and K. Aki, *ibid.*, p. 1669]. H. Kanamori [*ibid.* **69**, 1645 (1979)] simulated the 1857 earthquake by adding time-lagged discrete subevents whose ground motion was modeled using scaled data from the 1968 Borrego Valley **M** 6.7 earthquake. In each of these papers the dominant ground motion is due to the longer period waves, and the duration is primarily controlled by the time it takes the rupture to propagate from the hypocenter to the ends of the fault (fault length of 305 to 375 km).
10. P. Ehlig, in *Calif. Div. Mines Geol. Spec. Rep. 118* (1975), p. 177.
11. R. Yerkes *et al.*, *U.S. Geol. Surv. Prof. Pap. 420-A* (1965); T. Wright, in *Active Margin Basins: Am. Assoc. Pet. Geol. Mem.* **52**, 35 (1991).
12. D. Hadley and H. Kanamori, *Geol. Soc. Am. Bull.* **88**, 1469 (1977).
13. J. Vidale and D. Helmberger, *Bull. Seismol. Soc. Am.* **78**, 122 (1988); K. Yomogida and J. Etgen, *ibid.* **83**, 1325 (1993); R. Graves, *Geophys. Res. Lett.* **22**, 101 (1995).
14. A. Frankel, *Bull. Seismol. Soc. Am.* **83**, 1020 (1993).
15. With an average slip of 4.82 m, we calculate a seismic moment of 4.75 × 10^{20} Nm, giving a **M** 7.75 for the earthquake. The slip of 4.82 m is within the range of characteristic slip (4.5 ± 1.5 m) for earthquakes on the Mojave segment but is slightly larger than the characteristic slip (3.5 ± 1.0 m) on the San Bernardino segment (*2*). Similarly the stress drop σ for a long strike-slip fault with width, W, is given by $\sigma = (2/\pi)\mu(s/W)$ [L. Knopoff, *Geophys. J.* **1**, 44 (1958)] from which we estimate a stress drop of 69 bars—a value consistent with average earthquakes (H. Kanamori and D. Anderson, *Bull. Seismol. Soc. Am.* **65**, 1073 (1975).
16. H. Magistrale *et al.*, *Seismol. Res. Lett.* (abstr.) **65**, 39 (1994).
17. R. Yeats *et al.*, in *Santa Barbara and Ventura Basins*, A. Sylvester and G. Brown, Eds. (*Field Guide 64, Coast Geological Society*, Ventura, CA, 1988), pp. 133–144.
18. H. Kawase and K. Aki, *Bull. Seismol. Soc. Am.* **79**, 1361 (1989).
19. A propagating rupture is analogous to a double zipper. The first zipper, moving at the velocity of the rupture, unlocks the two sides of the fault. A second zipper arrives later to lock the two sides of the fault. In the time between the two zippers, the two sides of the fault move relative to each other. The total amount of relative movement before the second zipper locks the two sides is the offset or slip. The time it takes for the slip to occur is the rise time. The slip divided by the rise time is slip rate, that is how fast the slip occurs on the fault.
20. A. Levander, *Geophysics* **53**, 1425 (1988).
21. K. Olsen, thesis, University of Utah (1994).
22. C. Cerjan *et al.*, *Geophysics* **50**, 705 (1985); R. Clayton and B. Engquist, *Bull. Seismol. Soc. Am.* **71**, 1529 (1977).
23. The movement of the ground is three dimensional and can be completely described by examining it on three perpendicular axes. The natural choices are along the vertical and two horizontal directions. We have chosen the headings of 118° and 28°, parallel and perpendicular to the San Andreas, respectively, for positive horizontal ground velocity.
24. Y. Hisada *et al.*, in *Proc. Fourth Int. Conf. Seismic Zonation*, Stanford, CA (1991), vol. II, p. 245; A. Edelman and F. Vernon, unpublished report.
25. The amplitude of seismic waves can be attenuated by many different mechanisms, but the primary mechanisms are geometrical spreading and intrinsic attenuation. Geometrical spreading of the wavefront attenuates the amplitude as a direct result of conservation of energy. As the wavefront expands with distance from the source, the energy is spread over a greater surface area resulting in a smaller energy per unit area and accordingly a smaller amplitude. A simple approximation to geometrical spreading for body waves is: $A \propto 1/R$, where A is the amplitude of the wave and R is the distance between the source and the observer. For surface waves (Love and Rayleigh) the geometrical attenuation is approximately: $A \propto 1/\sqrt{R}$ so that surface waves decay more slowly than body waves. Intrinsic attenuation is the irreversible loss of wave energy due to internal friction as the waves propagate through the medium. The amplitude decay due to internal friction can be approximated by : $A \propto \exp(-\pi ft/Q)$ where f is frequency, t is the time it takes for a wave to travel from the source to the observer, and Q is a measure of the energy loss due to internal friction. We have omitted intrinsic attenuation in our simulation. However, comparison of observed seismic data from the 17 January 1994 **M** 6.7 Northridge event to an elastic simulation of the earthquake (*3*) suggests that intrinsic attenuation has limited effects on ground motion for frequencies less than 0.4 Hz, as used in this study.
26. The rupture directivity is an effect that modifies the energy in seismic waves depending on the angle between the observation point and the direction of rupture propagation [A. Ben-Menahem, *Bull. Seismol. Soc. Am.* **51**, 401 (1961)]. Directivity increases the energy in the direction the rupture propagates and decreases the energy in the back direction. A seismic pulse in the forward direction increases in amplitude and contracts in time; a seismic pulse in the back direction decreases in amplitude and expands in time. The directivity effect combined with the radiation pattern of S waves leads to large velocity pulses (on the order of 1.0 m/s) in the forward direction of earthquake ruptures [R. Archuleta and S. Hartzell, *Bull. Seismol. Soc. Am.* **71**, 939 (1981); R. Archuleta, *J. Geophys. Res.* **89**, 4559 (1984); (*4*)].
27. The cumulative kinetic energy for each gridpoint (x, y) on the surface is given by:

$$E_k(x,y) = \frac{1}{2}\rho(x,y)\int_0^T \dot{u}^2(x,y,t)dt$$

where k is the component of motion, ρ is the density, $\dot{u}(x,y,t)$ is the velocity seismogram, and T is the duration of the seismogram. The cumulative energy includes the amplitude and duration of the signal. The total energy is the sum of all three components: $E_{tot}(x,y) = E_{118}(x,y) + E_{28}(x,y) + E_V(x,y)$.
28. There are formulas for relating the height of structures with the period of the lowest-mode response. For example, with h(ft) = (period/0.035)$^{1.333}$ [*Uniform Building Code* (International Conference of Building Officials, Whittier, CA, 1988)], a 3.0-s period corresponds to a 115-m-high steel frame building. Such formulas serve as a guide; more flexible buildings or buildings made of different materials may be significantly shorter for a given period. For example, the Sherman Oaks building has a lowest-mode period of 3 s (0.33 Hz) but is 50.6 m high (13 stories) [Chapter 2, *Earthq. Spectra Suppl. C* **11**, 13 (1995)].
29. The classification of soils and rock in geotechnical engineering depends on the S wave velocity. A firm to hard rock has an average shear-wave speed greater than 700 m/s [R. Borcherdt, *Earthq. Spectra* **10**, 617 (1994)]. The lowest velocity in our model is 1.0 km/s (Table 2).
30. Many papers document the amplification of seismic waves due to local near-surface geology [for example, K. Aki, *Am. Soc. Civil Eng. Proc. Spec. Conf. Earthq. Eng. Soil Dyna.* **2**, 1 (1988)].

31. We are grateful to MIT's Earth Resources Laboratory for permission to use the nCUBE 2 parallel computer. We thank H. Magistrale for allowing us to use his 3D LA basin model and S. Day for advice on insertion of the double-couple source into the finite-difference scheme. This work was supported by the Southern California Earthquake Center (SCEC), USC 572726 through the NSF cooperative agreement EAR-8920136.

27 September 1995; accepted 14 November 1995

Reproduced with permission of the copyright owner. Further reproduction prohibited without permission.